

Analytic next-to-leading order electroweak corrections to Higgs boson pair production at high energies

Joshua Davies,^a Kay Schönwald,^b Matthias Steinhauser,^c Hantian Zhang^b

^a*Department of Mathematical Sciences, University of Liverpool, Liverpool, L69 3BX, UK*

^b*Theoretical Physics Department, CERN, 1211 Geneva 23, Switzerland*

^c*Institut für Theoretische Teilchenphysik, Karlsruhe Institute of Technology (KIT), Wolfgang-Gaede Straße 1, 76131 Karlsruhe, Germany*

ABSTRACT: We compute the complete next-to-leading order electroweak corrections to the form factors entering gluon-induced Higgs boson pair production. We consider the top quark contribution in the limit where the Mandelstam variables are much larger than all other scales involved in the process and compute about a hundred expansion terms in analytic form. They are used to obtain precise numerical results even for fairly low values of the transverse momentum of the Higgs boson. We show that these electroweak corrections at high energies are of the order of -10% . We also discuss the leading logarithmic corrections of the analytic expressions.

Contents

1	Introduction	1
2	Conventions	2
3	Technical details	3
4	Renormalization	6
5	Results	7
5.1	Analytic results	7
5.2	Construction of approximations	9
5.3	Numerical results	10
6	Conclusions and outlook	15

1 Introduction

Higgs boson pair production is the most promising process to probe the Higgs self-coupling in the Standard Model (SM) at the Large Hadron Collider (LHC). For this process, precise theoretical predictions are indispensable to interpret the experimental data. At the LHC, the dominant contribution to the cross section comes from the loop-induced gluon-fusion process $gg \rightarrow HH$ that receives large higher-order corrections [1–4].

In this context, next-to-leading order (NLO) two-loop electroweak (EW) corrections to $gg \rightarrow HH$ at high energies are of both theoretical and phenomenological interest. The high-energy behaviour of scattering amplitudes beyond logarithmic and leading power approximations is a state-of-the-art problem in quantum field theory, whose complexity further increases when the full electroweak sector of the SM is taken into account. The high-energy expansion of the $gg \rightarrow HH$ amplitudes will be particularly useful for studying the production of boosted Higgs bosons at the LHC [5], especially in the upcoming high-luminosity phase.

In the literature, there are a number of electroweak calculations available for $gg \rightarrow HH$. The leading Yukawa corrections have been first considered in the high-energy expansion [6] and the large top-mass limit [7]. The first electroweak calculation involving top-quarks, gauge and Higgs bosons has been performed in a large top-mass expansion [8], where five expansion terms in $1/m_t^2$ are presented. The complete electroweak corrections including all SM contributions have been computed numerically [9]. In particular, the contributions including Higgs self-couplings (and Yukawa) corrections have been computed with numerical approaches [10–12] and analytic expansions [13, 14]. Exact analytic results are available

for the factorizable electroweak contributions [15] and the light-quark electroweak contributions [16]. Combined results of Yukawa and light-quark contributions are also available in [17, 18]. Contributions from the quark-antiquark channel are available from Ref. [19].

In the QCD sector, the high-energy amplitudes have proven to be valuable for a number of phenomenologically important processes [20–27]. For example, a deep high-energy expansion for $gg \rightarrow HH$ [21, 22] has been successfully combined with the numerical approach [4] or forward-scattering expansions [28–31] to cover the full phase space for QCD corrections.

In this paper, we present the full analytic result for electroweak corrections in a deep high-energy expansion for $gg \rightarrow HH$ involving top quarks, gauge and Higgs bosons. We will show that our result can cover a large phase-space region, ranging from the high-energy limit to fairly low values of the Higgs boson transverse momentum. These results lead to negative corrections of the order of -10% at the partonic level.

The outline of this paper is as follows: In Section 2 we present our conventions, and in Section 3 we provide technical details on the computation of the Feynman diagrams and in particular on the implementation of the expansions. In Section 4 we describe the renormalization, for which we use the on-shell scheme. Results for the form factors are shown in Section 5 where we also discuss their high-energy structures and describe our approach to obtain Padé-improved approximations. We conclude in Section 6.

2 Conventions

We adopt the conventions of Section 2 of Ref. [14]. For convenience we repeat the most important formulae in the following.

We consider the process $g(q_1)g(q_2) \rightarrow H(q_3)H(q_4)$, where all momenta are incoming. The corresponding amplitude can be decomposed as a linear combination of two Lorentz structures with scalar coefficients \mathcal{M}_1 and \mathcal{M}_2 . The latter are in turn decomposed into “box” and “triangle” form factors as follows

$$\begin{aligned}\mathcal{M}_1 &= X_0 s (F_{\text{tri}1} + F_{\text{box}1}) , \\ \mathcal{M}_2 &= X_0 s F_{\text{box}2} ,\end{aligned}\tag{2.1}$$

where we have introduced

$$F_{\text{tri}1} = \frac{3m_H^2}{s - m_H^2} \left(F_{\text{tri}} + \frac{m_H^2}{s - m_H^2} \tilde{F}_{\text{tri}} \right).\tag{2.2}$$

Note that at leading order (LO) we have $\tilde{F}_{\text{tri}} = 0$. The prefactor in Eq. (2.1) is given by

$$X_0 = \frac{G_F \alpha_s(\mu)}{\sqrt{2} 4\pi},\tag{2.3}$$

where μ is the renormalization scale and G_F is the Fermi constant.

For this process, the Mandelstam variables are given by

$$s = (q_1 + q_2)^2, \quad t = (q_1 + q_3)^2, \quad u = (q_2 + q_3)^2,\tag{2.4}$$

with

$$q_1^2 = q_2^2 = 0, \quad q_3^2 = q_4^2 = m_H^2, \quad s + t + u = 2m_H^2. \quad (2.5)$$

One often either uses \sqrt{s} and the transverse momentum of the Higgs bosons in the center-of-mass frame, p_T , or \sqrt{s} and the scattering angle θ (also in the center-of-mass frame) in order to parametrize the phase space. The relations to the Mandelstam variables are given by

$$p_T^2 = \frac{ut - m_H^4}{s},$$

$$t = m_H^2 - \frac{s}{2} \left(1 - \cos \theta \sqrt{1 - \frac{4m_H^2}{s}} \right). \quad (2.6)$$

We define the perturbative expansion of the form factors as follows

$$F = F^{(0)} + \frac{\alpha_s(\mu)}{\pi} F^{(1,0)} + \frac{\alpha}{\pi} F^{(0,1)} + \dots, \quad (2.7)$$

where α_s is the strong coupling constant and α is the fine structure constant. $F^{(1,0)}$ represents the two-loop QCD corrections which are not discussed in this paper. Their high-energy expansion has been computed in Ref. [21, 22].

3 Technical details

Typical Feynman diagrams which contribute to the two-loop electroweak corrections are shown in Fig. 1. We want to stress that besides the one-particle irreducible (1PI) contributions to the two-loop amplitudes there are also one-particle reducible (1PR) contributions (which have been computed in Ref. [15]). As a subset of the latter we also include the so-called tadpole contributions, which are necessary to obtain a finite result (see Section 4).

We consider all sectors of the SM. However, we concentrate on the top quark-induced contributions since the light-quark contributions are known in analytic form from Ref. [16]. An exploratory study of the high-energy behaviour for the diagrams with a Higgs boson exchange has been presented in Ref. [6], where all fully-massive planar master integrals were computed. High-energy corrections for the subset of Feynman diagrams with non-zero top quark Yukawa and Higgs self couplings were considered in Ref. [14]. In this paper, deep analytic expansions for all fully-massive non-planar master integrals have been obtained.

A calculation of the complete NLO electroweak corrections with general gauge parameters has been performed in Ref. [8] in the large- m_t limit, where it was demonstrated that the gauge parameter dependence drops out for physical quantities. In the current paper we use the same set of diagrams but set all gauge parameters (γ , Z and W) to Feynman gauge. As a consequence, the neutral and charged Goldstone bosons have the same masses as the corresponding gauge bosons, Z and W . A different choice of the gauge parameters would introduce additional, but spurious, mass scales.

Our calculation involves several mass scales, which is currently too complicated to arrive at analytic results for the form factors. For this reason we perform several expansions:

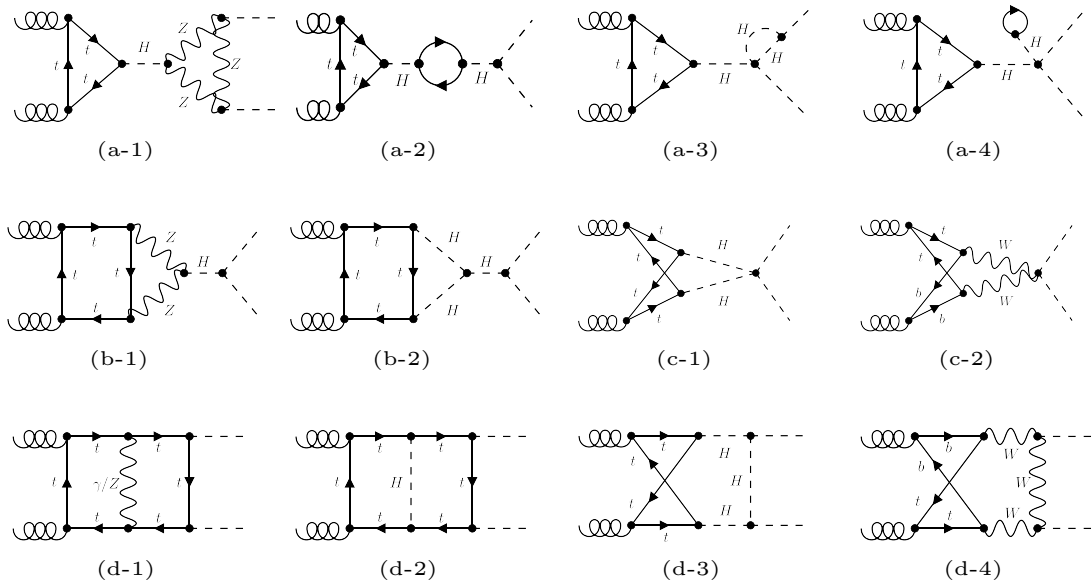


Figure 1: Sample Feynman diagrams contributing to the NLO electroweak corrections to $gg \rightarrow HH$. In the top, middle and bottom row, 1PR, triangle and box diagrams are shown. Note that (c-1) and (c-2) enter the box form factors since there is no Higgs boson propagator.

we perform Taylor expansions in the final-state Higgs boson mass and in the mass differences of the top quark mass m_t and the other boson masses in the loop diagrams. The resulting integrals are expanded in the high-energy limit, where the Mandelstam variables s and t are much larger than the top quark mass.

In the following we describe the computation of the 1PI two-loop diagrams. The Higgs boson mass appears in several places. Since we process them differently we distinguish them in the intermediate steps of our calculation. We denote the mass of the final-state Higgs bosons by m_H^{ext} , the one in the propagators inside loop diagrams by m_H^{int} , and the Higgs boson mass in the propagator of the triangle diagrams which is outside of the loop by m_H^{prop} . Furthermore, in the SM the Higgs boson mass appears in the expression for the Higgs boson self coupling λ . We denote it by m_H^λ thus have

$$\lambda = \frac{e^2(m_H^\lambda)^2}{8m_Z^2 c_w^2 s_w^2}, \quad (3.1)$$

where $e = \sqrt{4\pi\alpha}$, α is the fine structure constant, $c_w \equiv \cos(\theta_w)$ is the cosine of the weak mixing angle, and $s_w^2 \equiv 1 - c_w^2$.

Note that for the box diagrams, m_H^λ may have a different value to the “other” Higgs boson masses without affecting the renormalization of the amplitude. This is not the case for the triangle contributions; here we must identify $m_H^\lambda = m_H^{\text{prop}}$ for a complete renormalization. The values of m_H^{int} (which only appears at NLO) and m_H^{ext} (which is an external particle) can not interfere with the renormalization procedure. For numerical

evaluation in Section 5.3, we of course use the same values for m_H^{ext} , m_H^{int} , m_H^{prop} and m_H^λ , as given in Eq. 5.11.

Besides the Mandelstam variables s and t , the additional scales are the top quark mass m_t and the gauge boson masses m_Z and m_W . For the latter we also distinguish the masses in the couplings from those in the propagators inside loop diagrams, which we denote by m_Z^{int} and m_W^{int} , respectively. Note that for any given diagram there are at most two different masses present: m_t and one of the boson masses m_H^{int} , m_Z^{int} or m_W^{int} . Thus, for the generation of the form factors expressed in terms of master integrals we proceed as follows.

We use `qgraf` [32] for the generation of the amplitude, `tapir` [33] for the translation to FORM [34, 35] notation and the generation of auxiliary files for processing the integral topologies, and `exp` [36, 37] for the mapping of each Feynman diagram onto a minimal subset of the integral topologies from `tapir`.

The masses of the internally propagating bosons are expanded around m_t as a series in $\delta'_X = 1 - (m_X^{\text{int}}/m_t)^2$ with $X = H, Z, W$, see also Refs. [6, 14]. As a result, for the diagrams containing virtual Z or Higgs bosons, all internal lines have the same mass: m_t . These integral families have already been classified in Refs. [6, 14], where all relevant master integrals have been computed. For the diagrams with virtual W bosons we have both massive lines (with mass m_t) and massless lines which originate from the bottom quark propagators. The integral families correspond to those of the QCD corrections have been defined in Refs. [21, 22]. Deep expansions of the master integrals have been computed in Ref. [30]. Further technical details regarding calculations of master integrals can be found in Refs. [38, 39]. In the final results we switch to the expansion parameter $\delta_X = 1 - m_X^{\text{int}}/m_t$, since it shows better convergence properties (as e.g. described in Ref. [40]). We use the relation $\delta'_X = \delta_X(2 - \delta_X)$ and expand in δ_X up to the same order which we had for δ'_X .

We compute the amplitude using the in-house FORM code “`calc`”, which applies projectors to obtain the form factors, takes traces and expresses the final result in terms of scalar integrals of the integral families selected by `exp`. In this step we also perform the expansion of all boson propagators such that in the final results we have terms up to order δ_X^k . For our calculation we have $k = 3$, see also below. Note that there are no “mixed” terms in the δ_X expansion since Higgs, Z and W bosons never appear in the same Feynman diagram. At this point the scalar integrals depend on the variables $\{s, t, m_H^{\text{ext}}, m_t\}$; δ_X is only present in the integral coefficients.

The next step is to expand in the final state Higgs boson mass which is encoded in the relation of the external momenta, the Mandelstam variables and m_H^{ext} , see Eqs. (2.4) and (2.5). We perform the expansion of each scalar integral at the level of the integrands with the help of `LiteRed` [41, 42]. We generate FORM `Identify` statements which are applied to the summed expressions for the form factors. The remaining scalar integrals then depend only on $\{s, t, m_t\}$. The reduction to master integrals for the fully-massive families is performed with `Kira` [43–45]. We extend the tables which have been generated for the calculation performed in Ref. [14]. This part of the amplitude is expressed in terms of 168 master integrals, 28 of which are non-planar. For the QCD-like families we use the setup developed in Ref. [21, 22]. In particular, we use `FIRE` [46] for the reduction and

express the amplitude in terms of 161 master integrals, 30 of which are non-planar. The reduction tables are inserted into the amplitude using FORM. This must be programmed carefully, to avoid both generating overly-large terms and blowing up the total number of terms in the expressions.

Finally, we expand the amplitude in ϵ and for $m_t \rightarrow 0$ and insert the analytic high-energy expansion of all master integrals from Refs. [6, 14, 21, 22, 30]. This final stage of the computation is implemented efficiently in FORM by making use of Tablebases to store the ϵ and m_t expansion coefficients of the master integrals.

At this point we have obtained analytic expressions for the (bare) form factors with explicit dependence on $s, t, m_t, m_H^{\text{ext}}$ and δ_X . We have computed expansion terms up to m_t^{108} , $(m_H^{\text{ext}})^4$ and δ_X^3 , and for $(m_H^{\text{ext}})^0$ also δ_X^4 . Due to the deep expansion in m_t the expressions are quite large; they total around 6.5 GB of gzip-compressed files.

In this work, we use **Mathematica** for the numerical evaluation at 200 digits or more, which takes about half an hour (with some dependence on the phase-space point). For the calculation of hadronic cross sections, it is important to export these expressions to **Fortran** or **C** which will lead to a significant reduction of the runtime. However, this must be done carefully so that the compilation time is no more than a few hours.

The next step is to renormalize the form factors, followed by their numerical evaluation and Padé approximation procedure. We discuss the details of these parts of the calculation in the following sections.

4 Renormalization

For the NLO electroweak corrections there is no real-radiation contribution and thus all $1/\epsilon$ poles are of ultraviolet origin. They are removed after the renormalization of an independent set of quantities. In our case we choose the W , Z and Higgs boson masses, the top quark mass and the electric charge which is related to the fine structure constant via $e = \sqrt{4\pi\alpha}$. We adopt the on-shell renormalization scheme and introduce the Z factors as follows

$$\begin{aligned}
 e^0 &= Z_e e, \\
 m_t^0 &= Z_{m_t} m_t, \\
 m_W^0 &= Z_{m_W} m_W, \\
 m_Z^0 &= Z_{m_Z} m_Z, \\
 m_H^0 &= Z_{m_H} m_H,
 \end{aligned}
 \tag{4.1}$$

where the superscript “0” indicates bare quantities. In addition to the parameters in Eq. (4.1) we have to renormalize the wave function of the Higgs boson

$$H^0 = \sqrt{Z_H} H,
 \tag{4.2}$$

where H is the Higgs boson field. All Z factors can be computed from two-point functions; explicit analytic expressions can, e.g., be found in Refs. [47, 48].

Let us also stress that our NLO electroweak form factors do not have an explicit dependence on the renormalization scale since all parameters are renormalized in the on-shell scheme.

We consistently include tadpole contributions in all parts of our calculation, i.e., in the bare two-loop amplitude and the Z factors. This prescription is equivalent to the so-called *Fleischer–Jegerlehner tadpole scheme* [49]. Alternative options to treat the tadpole contributions are discussed, e.g., in Ref. [50].

We renormalize the box and triangle contributions independently. In the case of the box contribution, at two-loop order there are only 1PI Feynman diagrams (see Fig. 1), and contributions from diagrams where one-loop tadpoles are attached to the (virtual) top quark propagators. The identical tadpole contributions are present in the on-shell renormalization constant Z_{mt} . Thus they exactly cancel in the on-shell scheme and finite results for $F_{\text{box}1}$ and $F_{\text{box}2}$ are obtained from parameter and wave function renormalization (as detailed above) by considering only 1PI contributions. This is different in the case of the triangle contribution where further types of tadpole diagrams arise, see Fig. 1. Furthermore, there are various 1PR diagrams with one-loop corrections to the Higgs boson propagator or one-loop vertex corrections to the final-state triple-Higgs boson vertex. We find it convenient to sum all 1PI and 1PR contributions to the two-loop amplitude and the renormalization constants and proceed with the renormalization as described above. This leads to a finite results for $F_{\text{tri}1}$.

In the counterterm contribution we use for all (one-loop) Z factors exact (i.e. non-expanded) results. Since the Z factors contain $1/\epsilon$ poles we need the one-loop amplitudes including linear terms in ϵ . For the triangle diagrams the (exact) results can be found in Ref. [15]. They contain at most tri-logarithms. It is possible to compute the $\mathcal{O}(\epsilon)$ terms of the box contributions, however the analytic expressions are rather cumbersome. For this reason we use the deep high-energy expansion of the one-loop box amplitudes from the calculation of the QCD corrections in Ref. [30] (see also Ref. [14]).

In a next step we transform our results into the so-called G_μ scheme where the fine structure constant α is replaced by the Fermi constant G_F . For explicit expressions we refer, e.g., to Section 5.1.1 of Ref. [48]. The transformation to the G_μ scheme introduces the quantity Δr [51]. For an explicit result, see Eq. (423) of Ref. [48]. In our numerical evaluation we do not expand Δr but evaluate it exactly, and we evaluate the Z factors similarly. Note that $F^{(0,1)}$ in Eq. (2.7) is already defined in the G_μ scheme.

5 Results

5.1 Analytic results

For convenience we provide explicit analytic results for the leading non-vanishing terms of the LO form factors. They are given by

$$F_{\text{tri}}^{(0)} = \frac{2m_t^2}{s} \left[4 - l_{ms}^2 \right] + \mathcal{O} \left(\frac{m_t^4}{s^2} \right),$$

$$F_{\text{box}1}^{(0)} = \frac{4m_t^2}{s} \left[2 + \frac{m_H^2}{s} \left((l_{1ts} - l_{ts})^2 + \pi^2 \right) \right] + \mathcal{O} \left(\frac{m_t^4}{s^2}, \frac{m_H^4}{s^2} \right),$$

$$\begin{aligned}
F_{\text{box}2}^{(0)} = & \frac{2m_t^2}{st(s+t)} \left[-l_{1ts}^2 (s+t)^2 - l_{ts}^2 t^2 - \pi^2 (s^2 + 2st + 2t^2) + \frac{2m_H^2}{s(s+t)} \left(l_{1ts}^2 s(s+t)^2 \right. \right. \\
& + \pi^2 s^3 + 2s^2 t (-2l_{ms} + l_{ts} + \pi^2 - 4) - st^2 (8l_{ms} + (l_{ts} - 2)l_{ts} + 16) \\
& \left. \left. - 4(l_{ms} + 2)t^3 \right) \right] + \mathcal{O} \left(\frac{m_t^4}{s^2}, \frac{m_H^4}{s^2} \right), \tag{5.1}
\end{aligned}$$

where

$$l_{ms} = \log \left(\frac{m_t^2}{s} \right) + i\pi, \quad l_{ts} = \log \left(-\frac{t}{s} \right) + i\pi, \quad l_{1ts} = \log \left(1 + \frac{t}{s} \right) + i\pi. \tag{5.2}$$

At two-loop order the form factors have a more complicated structure. However, the leading logarithmic contributions in $\log(m_t^2/s)$ are sufficiently compact. For the box form factors they are given for $m_t \rightarrow 0$ and $m_H = 0$ by

$$F_{\text{box}1}^{(0,1)} = \frac{m_W^4}{s^2 c_w^6 s_w^2} \left[l_{ms}^2 \frac{36c_w^6 + 32c_w^4 - 40c_w^2 + 17}{36} \left(l_{1ts}^2 + l_{ts}^2 - 2l_{1ts}l_{ts} + \pi^2 - 4 \right) \right] + \dots, \tag{5.3}$$

$$\begin{aligned}
F_{\text{box}2}^{(0,1)} = & \frac{m_W^4}{s^2 c_w^6 s_w^2} \left[l_{ms}^3 \frac{36c_w^6 + 32c_w^4 - 40c_w^2 + 17}{27} + l_{ms}^2 \left(-\frac{2}{9} \delta_Z (32c_w^4 - 40c_w^2 + 17) \right. \right. \\
& - 8 \delta_W c_w^6 + \frac{36c_w^6 + 32c_w^4 - 40c_w^2 + 17}{36t(s+t)} \left(l_{1ts}^2 (s+t)^2 - 2l_{1ts}t(s+t) - 2l_{ts}t(s+t) \right. \\
& \left. \left. \left. + l_{ts}^2 t^2 + \pi^2 (s^2 + 2st + 2t^2) \right) \right) \right] + \dots, \tag{5.4}
\end{aligned}$$

where the ellipsis stand for higher order terms in m_t and m_H and $\delta_{W/Z} = 1 - m_{W/Z}/m_t$. We note that the counterterms do not contribute to the results shown in Eqs. (5.3) and (5.4); they come exclusively from the two-loop diagrams.

We observe that the leading term for $F_{\text{box}1}$ is a quadratic logarithm, whereas $F_{\text{box}2}$ has a cubic contribution. Note that in the LO expression shown in Eq. (5.1) $F_{\text{box}1}$ has no $\log(m_t^2/s)$ terms at $\mathcal{O}(m_t^2)$ or $\mathcal{O}(m_H^2)$ and the linear logarithms of $F_{\text{box}2}$ are suppressed by m_H^2/s . The LO triangle form factor has a quadratic $\log(m_t^2/s)$ contribution which is suppressed at high energies by a factor of m_H^2/s due to the s -channel Higgs boson propagator. It is also interesting to remark that $F_{\text{box}2}^{(0,1)}$ has $\log^2(m_t^2/s)$ terms which are proportional to δ_W or δ_Z . There are no terms proportional to δ_H in the leading m_t^0 contribution, which might provide a reason for the smallness of the Yukawa and Higgs self coupling contributions at high energies, as observed in Ref. [12, 14].

For further analytic expressions we refer to the ancillary files [52] where we provide five expansion terms in the high-energy limit. Deeper expansions are available on request.

The generic structure of the high-energy expansion of the form factors has the form

$$F = \sum_{n=-4}^{108} \sum_{i=0}^2 \sum_{k_W=0}^4 \sum_{k_Z=0}^4 \sum_{k_H=0}^4 c_{nik_W k_Z k_H} m_t^n (m_H^{\text{ext}})^{2i} \delta_W^{k_W} \delta_Z^{k_Z} \delta_H^{k_H}, \tag{5.5}$$

where negative powers in m_t are only present for $i > 0$. Furthermore, there is the additional constraint that $k_W + k_Z + k_H \leq 3$ for $i = 1, 2$ and $k_W + k_Z + k_H \leq 4$ for $i = 0$. Since there are no “mixed” contributions in the δ_X expansions at most one of the indices k_W, k_Z, k_H may be non-zero. For convenience we perform the rescaling

$$\begin{aligned}\delta_W^{k_W} &\rightarrow \delta \delta_W^{k_W}, \\ \delta_W^{k_Z} &\rightarrow \delta \delta_Z^{k_Z}, \\ \delta_W^{k_H} &\rightarrow \delta \delta_H^{k_H},\end{aligned}\tag{5.6}$$

and count in the following the powers of δ . The coefficients $c_{nik_W k_Z k_H}$ in Eq. (5.5) depend on t/s and $\log(m_t^2/s)$.

5.2 Construction of approximations

In the following, we describe our procedure to construct approximations. First, we fix the maximal powers of δ and $(m_H^{\text{ext}})^2$ and insert the numerical values for $\delta_W, \delta_Z, \delta_H$ and m_H^{ext} . We then specify the phase-space point (i.e. the values of s and t). This leads to an expansion in m_t . Next we insert the numerical value for m_t if it appears in the argument of logarithms. Then we rescale odd and even power of m_t according to $m_t^{2k} \rightarrow m_t^{2k} x^k$ and $m_t^{2k-1} \rightarrow m_t^{2k-1} x^k$ and insert also here the numerical value for m_t . As a result we obtain a polynomial of degree $N = 54$ in x . Afterwards we construct a Padé approximant of the form

$$[n/m](x) = \frac{a_0 + a_1 x + \dots + a_n x^n}{1 + b_1 x + \dots + b_m x^m},\tag{5.7}$$

where $n + m = N$. We can vary the parameters n and m and we can also choose $N < 54$. This provides the possibility to generate a large number of Padé approximants which allows us to determine a central value and an uncertainty interval. This procedure is performed separately for each phase-space point. More details can be found in Refs. [4, 53].

Whereas in the high-energy limit we can construct a deep expansion in m_t , we only have a few terms in the expansion in δ and the final-state mass m_H^{ext} . To improve convergence in these parameters, sum acceleration techniques can be useful. We use the so-called *Aitken extrapolation* (see, Ref. [54]) and proceed as follows: The starting point is an expansion of the form

$$A = \sum_{i=0}^{\infty} A_i y^i,\tag{5.8}$$

where in our case y tags either the expansion in δ or in $(m_H^{\text{ext}})^2$. The A_i correspond to the Padé approximations based on the specified input and expansion depths, which are described below. We then construct the partial sums

$$A^{(k)} = \sum_{i=0}^k A_i y^i, \quad k = 0, 1, \dots, k_{\text{max}},\tag{5.9}$$

where for the expansion in $(m_H^{\text{ext}})^2$ we have $k_{\text{max}} = 3$, while we have $k_{\text{max}} = 4$ for the expansion in δ .¹ These partial sums are used to obtain the new approximation:

$$A_{\text{acc}}^{(n)} = \frac{A^{(n)}A^{(n+2)} - (A^{(n+1)})^2}{A^{(n)} - 2A^{(n+1)} + A^{(n+2)}}. \quad (5.10)$$

It is interesting to note that $A_{\text{acc}}^{(n)}$ corresponds to the $[n + 1/1]$ Padé approximant.

For the expansion in δ we can construct the accelerated results $A_{\text{acc}}^{(0)}$, $A_{\text{acc}}^{(1)}$ and $A_{\text{acc}}^{(2)}$. We can compare $A_{\text{acc}}^{(0)}$ and $A_{\text{acc}}^{(1)}$, which only include expansions up to δ^2 or δ^3 , respectively, to results which include δ^3 or δ^4 terms without any acceleration. We estimate the final uncertainty of the δ expansion using the difference between our best “raw” and accelerated results.

In principle we could also consider sum acceleration in m_H^{ext} . However, as we will see below, the expansion in m_H^{ext} converges sufficiently quickly that the application of sum acceleration is not necessary.

5.3 Numerical results

In this section we present numerical results for the form factors and the squared partonic amplitude. We use the following input values [55]

$$\begin{aligned} G_F &= 1.166378 \times 10^{-5} \text{ GeV}, \\ m_H &= 125.2 \text{ GeV}, \\ m_Z &= 91.19 \text{ GeV}, \\ m_W &= 80.37 \text{ GeV}, \\ m_t &= 172.57 \text{ GeV}, \end{aligned} \quad (5.11)$$

and introduce the coupling (e.g. in Eq. (2.7))

$$\alpha_{G_\mu} = \frac{\sqrt{2}}{\pi} G_F m_W^2 \left(1 - \frac{m_W^2}{m_Z^2}\right), \quad (5.12)$$

which is our expansion parameter in the G_μ scheme. The squared matrix element can be perturbatively expanded as

$$\mathcal{U} = \frac{1}{16} (|\mathcal{M}_1|^2 + |\mathcal{M}_2|^2) = \frac{(X_0 s)^2}{16} \left(\mathcal{U}^{(0)} + \frac{\alpha_s(\mu)}{\pi} \mathcal{U}^{(1,0)} + \frac{\alpha}{\pi} \mathcal{U}^{(0,1)} + \dots \right), \quad (5.13)$$

which we use to define the ratio

$$r_{\text{EW}} = \frac{\alpha}{\pi} \frac{\mathcal{U}^{(0,1)}}{\mathcal{U}^{(0)}}, \quad (5.14)$$

which quantifies the size of the NLO corrections at the partonic level. In the results discussed below we use for the LO term in the denominator of Eq. (5.14) the expanded expressions. For all phase-space points which are considered in this paper this provides an excellent approximation to the exact results.

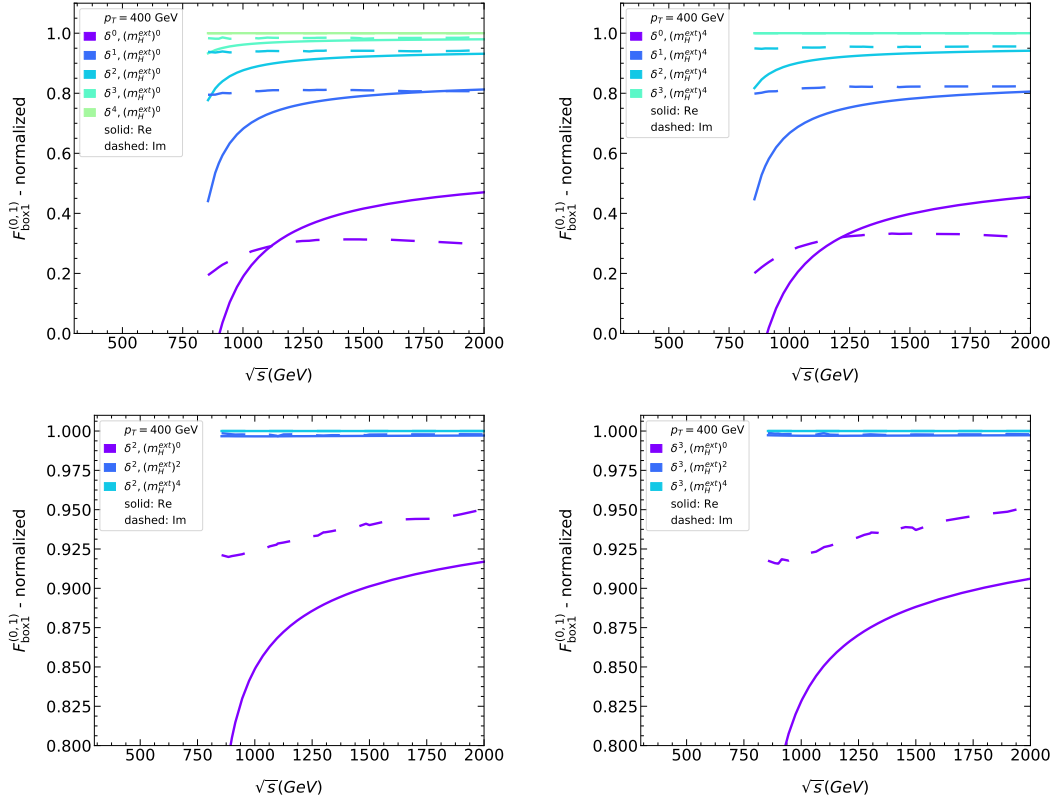


Figure 2: Ratio of various δ and m_H expansion terms normalized to the highest available approximation for $F_{\text{box}1}^{(0,1)}$. Results for the real and imaginary parts are shown as solid and dashed lines, respectively. The expansion depths given in the legend indicate the expansion terms which are used for the construction of the Padé approximation. Here “ $\delta^n, (m_H^{\text{ext}})^m$ ” means that all expansion terms δ^k and $(m_H^{\text{ext}})^l$ with $k \leq n$ and $l \leq m$ are included. Top row: Fixed expansion depth in m_H . Bottom row: Fixed expansion depth in δ .

In the following, we describe Padé results which have been obtained using expansion depths between $(m_t^2)^{46}$ and $(m_t^2)^{54}$. Furthermore, we include approximations up to $(m_H^{\text{ext}})^4$ and δ^4 . Coefficients which are not available (i.e. $(m_H^{\text{ext}})^2\delta^4$ and $(m_H^{\text{ext}})^4\delta^4$) are set to zero. Their numerical effect is expected to be small since the quartic m_H^{ext} terms are, in general, of the order of 1% or smaller, see below for more details.

In Figs. 2 and 3 we discuss the quality of the δ and m_H^{ext} expansions. In Fig. 2 we show results for $F_{\text{box}1}^{(0,1)}$ for $p_T = 400$ GeV. In the different panels we either vary the expansion depth in δ (top row) or m_H^{ext} (bottom row) and normalize the results in each case to the highest available approximation. We observe a good convergence of the δ expansion; in each step the distance to the next expansion order is reduced by about a factor of two. The δ^3 term induces a shift below 10% (except for smaller values of \sqrt{s}) and the δ^4 term,

¹We set the expansion terms of $O(\delta^4(m_H^{\text{ext}})^i)$, $i > 0$ to 0. The justification for this procedure is discussed in Sec. 5.3.

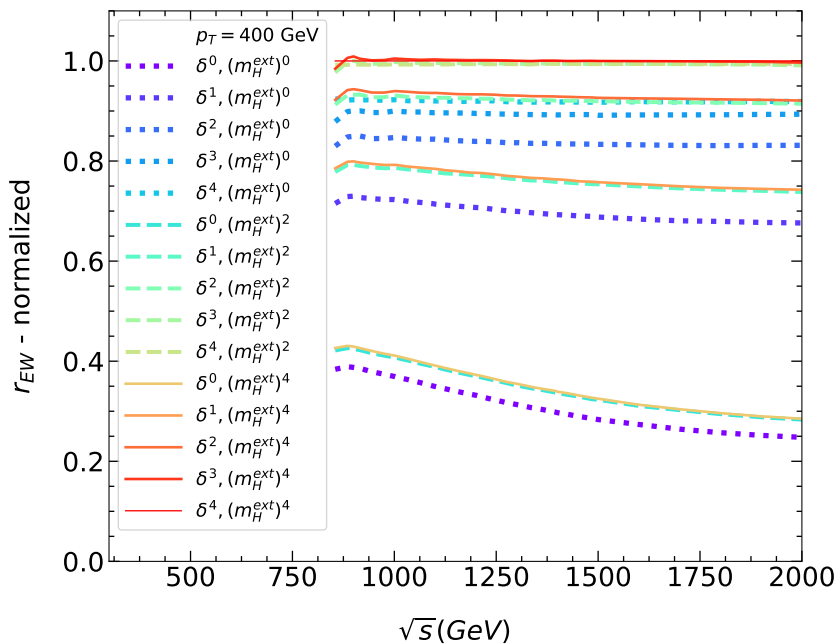


Figure 3: r_{EW} for various δ and m_H expansion terms normalized to highest available approximation for $p_T = 400$ GeV. For details concerning the meaning of the legend we refer to the caption of Fig. 2.

which is available for $m_H^{\text{ext}} = 0$, below 5%.

The convergence in m_H^{ext} is even faster, as can be seen from the panels in the bottom row of Fig. 2. Here we conclude that the quadratic terms in m_H^{ext} are of the order of 10% and the quartic terms are at the 1% level or below.

From the observed convergence pattern we can estimate the size of the missing m_H^{ext} terms at quartic order in δ . For the $\delta^4(m_H^{\text{ext}})^2$ [$\delta^4(m_H^{\text{ext}})^4$] terms we obtain $5\% \cdot 10\% = 0.5\%$ [$5\% \cdot 1\% = 0.05\%$] as compared to the known expansion terms. In our numerical analysis we will set these missing expansion terms to zero and assign to our final result a conservative uncertainty estimate of $\pm 1\%$.

In Fig. 3 we test our assumption for r_{EW} . We choose again $p_T = 400$ GeV. The dotted (blueish), dashed (greenish) and solid (reddish) curves show the δ expansion in case no, quadratic, or quartic m_H^{ext} terms are included in the computation of r_{EW} . In each case we construct five approximations which differ in the expansion depth in δ . In total 15 different approximations are shown in Fig. 3. All results are normalized to the approximation which includes $\delta^4(m_H^{\text{ext}})^4$ terms.² We observe a similar convergence pattern as in Fig. 2. In particular, the dashed and solid curves, which correspond to the same δ expansion, almost lie on top of each other indicating that the quartic m_H^{ext} terms are below 1%. Furthermore, the curves which belong to $\delta^3(m_H^{\text{ext}})^2$, $\delta^4(m_H^{\text{ext}})^2$ and $\delta^3(m_H^{\text{ext}})^4$ are very close to reference

²Note that this approximation contains all expansion terms δ^n and $(m_H^{\text{ext}})^m$ with $n \leq 3$ and $m \leq 4$, and the $\delta^4(m_H^{\text{ext}})^0$ term. However, the (numerically small) expansion terms $\delta^4(m_H^{\text{ext}})^2$ and $\delta^4(m_H^{\text{ext}})^4$ are set to zero, as described above.

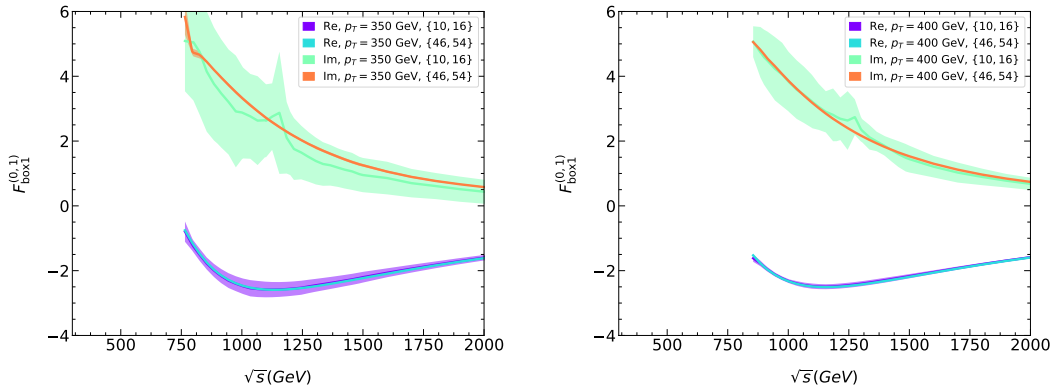


Figure 4: Real and imaginary parts of $F_{\text{box1}}^{(0,1)}$ for $p_T = 350$ GeV and $p_T = 400$ GeV as a function of \sqrt{s} for different expansion depth in m_t used for the Padé approximation, as indicated in the legend: $\{n, m\}$ means that for the construction of the Padé approximation at most expansions up to $(m_t^2)^m$ and at least up to $(m_t^2)^n$ are taken into account.

line at “1”, which supports our estimate that the higher order expansion terms in δ and m_H^{ext} are below a $\pm 1\%$ correction.

We observe a very similar convergence pattern for all values of $p_T \gtrsim 300$ GeV. This suggests the assignment of a total uncertainty of $\pm 1\%$ to the squared NLO matrix element when it is used as input for the hadronic cross sections. This estimate is further backed by the sum acceleration introduced in Section 5.2. We use sum acceleration for the expansion in δ , since it shows the slower overall convergence. We observe that $A_{\text{acc}}^{(0)}$, where no δ^3 terms enter, reproduces our nominal result including δ^3 terms within about 5%. Similarly, $A_{\text{acc}}^{(1)}$ reproduces the nominal result including δ^4 terms to order 1%. Furthermore, we observe that the difference between our nominal best approximation and $A_{\text{acc}}^{(2)}$ is below 1%, which again supports the conservative uncertainty estimate of 1% for r_{EW} .

Next we discuss the dependence on expansion depth in m_t . In Fig. 4 we show the real and imaginary parts of $F_{\text{box1}}^{(0,1)}$ for two different values of p_T , as a function of \sqrt{s} . In each case we show three curves and their associated uncertainty bands, which are all based on expansions up to δ^4 and m_H^2 but differ in the highest power in m_t used for the construction of the Padé-improved result, as indicated in the legend. We observe sizeable uncertainty bands for the approximations containing at most m_t^{32} terms, in particular for the imaginary part. The uncertainty is reduced substantially once we allow terms up to m_t^{108} terms. The latter is completely contained within the uncertainty band of the lowest approximation.

Here we note that at some phase-space points, which correspond to certain values of t , the m_t expansion does not converge in a way which leads to unstable Padé approximations. In these cases we use the $t \leftrightarrow u$ symmetry of the amplitude to provide an alternative, stable, evaluation.

In Figs. 5 and 6 we show NLO form factors $F_{\text{tri1}}^{(0,1)}$, $F_{\text{box1}}^{(0,1)}$ and $F_{\text{box2}}^{(0,1)}$ for fixed p_T or fixed \sqrt{s} , respectively. In all cases we show the highest available approximation which includes δ^4 and $(m_H^{\text{ext}})^4$ terms, together with the corresponding uncertainty band from the Padé

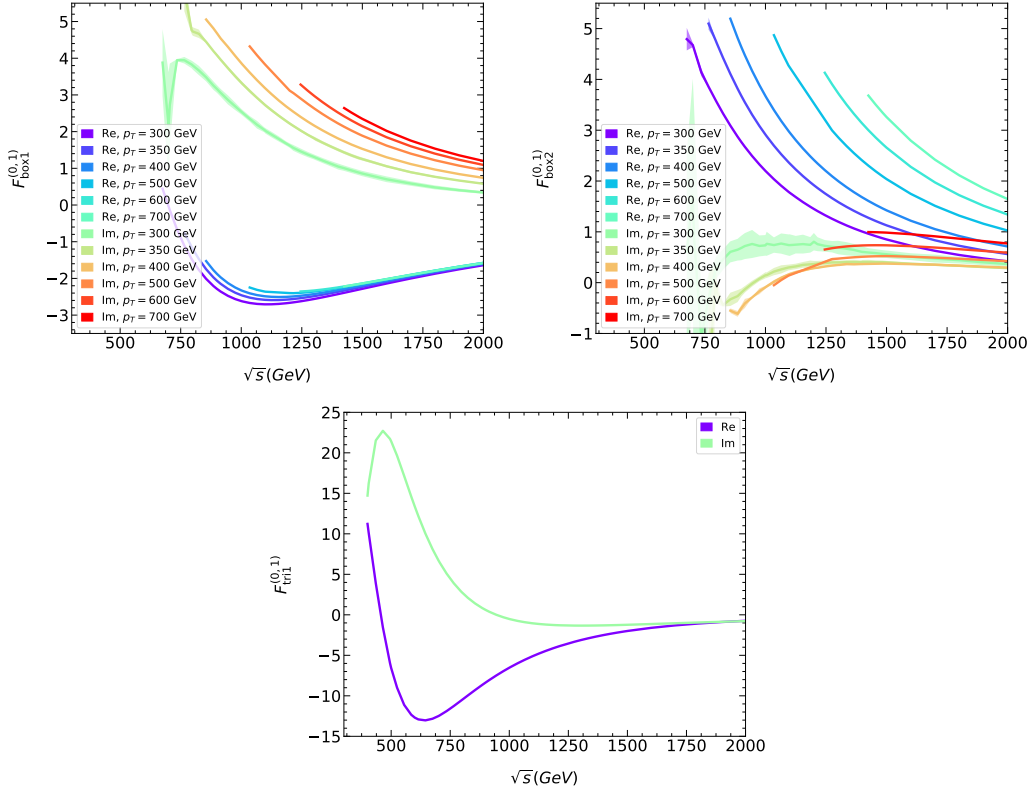


Figure 5: $F_{\text{box}1}$, $F_{\text{box}2}$ and $F_{\text{tri}1}$ as a function of \sqrt{s} for fixed p_T . Note that the triangle form factor is independent of p_T .

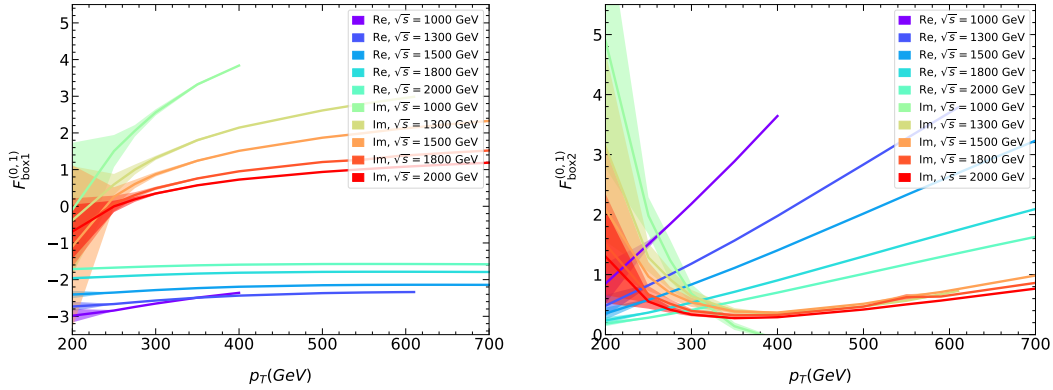


Figure 6: $F_{\text{box}1}$ and $F_{\text{box}2}$ as a function of p_T for fixed \sqrt{s} .

procedure.³ This band is only visible for $p_T \lesssim 350$ GeV and only for lower values of \sqrt{s} as can be seen in Fig. 5. It is, in general, more pronounced for the imaginary parts than for the real parts. From Fig. 6 we observe that for $p_T \gtrsim 350$ GeV the uncertainty induced by the Padé approximation is well below the uncertainty due to the truncated expansion in δ

³The estimated $\pm 1\%$ uncertainty from the truncation in δ and m_H^{ext} is not shown.

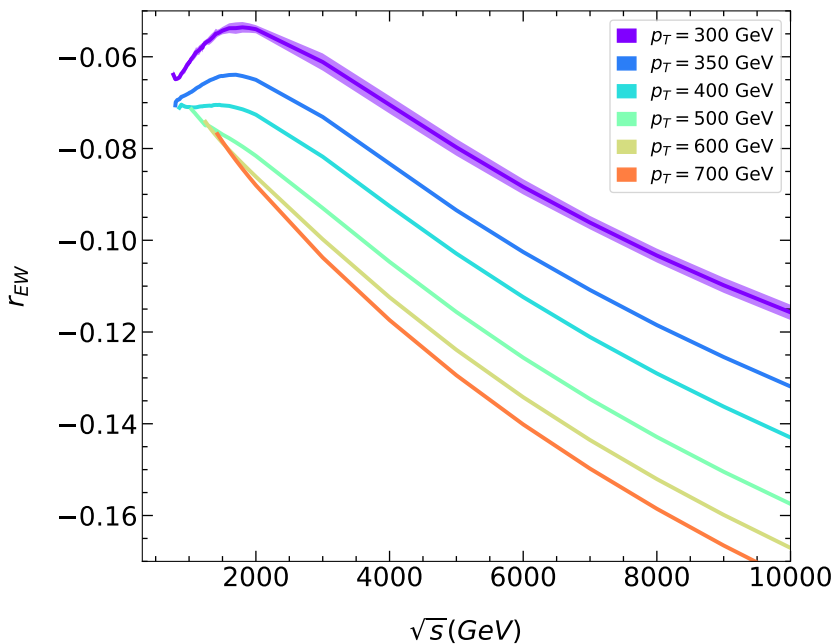


Figure 7: r_{EW} for various values of p_T as a function of \sqrt{s} . The plots show the same data for different ranges of \sqrt{s} on the x axis.

and m_H .

In Fig. 7, we show the ratio r_{EW} for fixed values of p_T as a function of \sqrt{s} which we extend up to 10 TeV. For each curve we use the highest available approximation and show, besides the central value, also the uncertainty bands as obtained from the Padé approximation. These are only visible for $p_T \lesssim 300$ GeV. The result for r_{EW} shows a more stable behaviour than for the individual (box) form factors. This can be explained by the dominance of the triangle form factors for smaller value of \sqrt{s} . For larger \sqrt{s} the approximations for the box form factors are stable for all p_T values shown in Fig. 7. The partonic quantity r_{EW} is negative and of the order of -10% , which is in agreement with the observations from Ref. [9] for the hadronic invariant mass or p_T distribution.

6 Conclusions and outlook

In this work, we compute NLO electroweak corrections to Higgs boson pair production in gluon fusion. We consider the top quark-induced contributions in the high-energy limit. Since we include all sectors of the Standard Model, several mass scales are involved in the computation. We identify certain hierarchies that allow us to perform nested expansions in several small parameters. In particular, we assume that the mass of the Higgs boson in the final state is small as compared to the top quark mass. Furthermore, we expand in mass differences in case several distinct masses appear inside the loop diagrams. Most importantly, we perform a deep expansion with more than 100 expansion terms around the high-energy limit. The calculation of the electroweak corrections is much more challenging

than in the QCD case; consequently, the intermediate and final expressions are considerably larger.

From the convergence properties of our results we estimate that the truncation uncertainty, dominated by the mass-difference expansion, is about $\pm 1\%$ of the two-loop corrections, which is well below the scale uncertainty from NLO QCD corrections. A systematic improvement is possible by computing more terms in the δ and m_H^{ext} expansion, which might be a challenging task from the computational point of view.

In the limiting case of massless external Higgs bosons, the leading high-energy expansion of the two-loop form factors starts at $(m_t^2/s)^0$, while at one loop the leading term starts at $(m_t^2/s)^1$. At NLO we observe a quadratic and cubic logarithm as the leading contribution for $F_{\text{box}1}$ and $F_{\text{box}2}$, respectively.

Our analytic results are explicit in all input parameters, allowing for a flexible use of the form factors and straightforward numerical evaluation. The results obtained in this paper cover the phase space for $p_T \gtrsim 350$ GeV and lead to corrections of the order of -10% at the partonic level in the high-energy limit. The high-energy results serve as cross check for other calculations, e.g., those based on numerical approaches (see, e.g., Refs. [9, 12]). Furthermore, it is expected that in combination with the forward limit expansion, the entire phase space can be covered as in the case of QCD (see, e.g., Ref. [31]).

Low-order expansions of our results are available from [52], and deep expansions are available upon request. Our results will be made public in the context of `ggxy` [31], which provides a framework to compute hadronic cross sections and distributions for gluon-induced processes.

Acknowledgements

This work is supported by the Deutsche Forschungsgemeinschaft (DFG, German Research Foundation) under grant 396021762 — TRR 257 “Particle Physics Phenomenology after the Higgs Discovery”. The work of J. D. is supported by STFC Consolidated Grant ST/X000699/1. K.S. and H.Z. are supported by the European Union under the Marie Skłodowska-Curie Actions (MSCA) Grants 101204018 and 101202083. We thank Marco Vitti for feedback on the manuscript.

References

- [1] S. Borowka, N. Greiner, G. Heinrich, S. P. Jones, M. Kerner, J. Schlenk et al., *Higgs Boson Pair Production in Gluon Fusion at Next-to-Leading Order with Full Top-Quark Mass Dependence*, *Phys. Rev. Lett.* **117** (2016) 012001 [[1604.06447](#)].
- [2] S. Borowka, N. Greiner, G. Heinrich, S. P. Jones, M. Kerner, J. Schlenk et al., *Full top quark mass dependence in Higgs boson pair production at NLO*, *JHEP* **10** (2016) 107 [[1608.04798](#)].
- [3] J. Baglio, F. Campanario, S. Glaus, M. Mühlleitner, M. Spira and J. Streicher, *Gluon fusion into Higgs pairs at NLO QCD and the top mass scheme*, *Eur. Phys. J. C* **79** (2019) 459 [[1811.05692](#)].

- [4] J. Davies, G. Heinrich, S. P. Jones, M. Kerner, G. Mishima, M. Steinhauser et al., *Double Higgs boson production at NLO: combining the exact numerical result and high-energy expansion*, *JHEP* **11** (2019) 024 [[1907.06408](#)].
- [5] ATLAS collaboration, *Search for pair production of boosted Higgs bosons via vector-boson fusion in the bb^-bb^- final state using pp collisions at $s=13\text{TeV}$ with the ATLAS detector*, *Phys. Lett. B* **858** (2024) 139007 [[2404.17193](#)].
- [6] J. Davies, G. Mishima, K. Schönwald, M. Steinhauser and H. Zhang, *Higgs boson contribution to the leading two-loop Yukawa corrections to $gg \rightarrow HH$* , *JHEP* **08** (2022) 259 [[2207.02587](#)].
- [7] M. Mühlleitner, J. Schlenk and M. Spira, *Top-Yukawa-induced corrections to Higgs pair production*, *JHEP* **10** (2022) 185 [[2207.02524](#)].
- [8] J. Davies, K. Schönwald, M. Steinhauser and H. Zhang, *Next-to-leading order electroweak corrections to $gg \rightarrow HH$ and $gg \rightarrow gH$ in the large- m_t limit*, *JHEP* **10** (2023) 033 [[2308.01355](#)].
- [9] H.-Y. Bi, L.-H. Huang, R.-J. Huang, Y.-Q. Ma and H.-M. Yu, *Electroweak Corrections to Double Higgs Production at the LHC*, *Phys. Rev. Lett.* **132** (2024) 231802 [[2311.16963](#)].
- [10] S. Borowka, C. Duhr, F. Maltoni, D. Pagani, A. Shivaaji and X. Zhao, *Probing the scalar potential via double Higgs boson production at hadron colliders*, *JHEP* **04** (2019) 016 [[1811.12366](#)].
- [11] H. T. Li, Z.-G. Si, J. Wang, X. Zhang and D. Zhao, *Improved constraints on Higgs boson self-couplings with quartic and cubic power dependencies of the cross section**, *Chin. Phys. C* **49** (2025) 023107 [[2407.14716](#)].
- [12] G. Heinrich, S. Jones, M. Kerner, T. Stone and A. Vestner, *Electroweak corrections to Higgs boson pair production: the top-Yukawa and self-coupling contributions*, *JHEP* **11** (2024) 040 [[2407.04653](#)].
- [13] W. Bizoń, U. Haisch and L. Rottoli, *Constraints on the quartic Higgs self-coupling from double-Higgs production at future hadron colliders*, *JHEP* **10** (2019) 267 [[1810.04665](#)].
- [14] J. Davies, K. Schönwald, M. Steinhauser and H. Zhang, *Analytic next-to-leading order Yukawa and Higgs boson self-coupling corrections to $gg \rightarrow HH$ at high energies*, *JHEP* **04** (2025) 193 [[2501.17920](#)].
- [15] H. Zhang, K. Schönwald, M. Steinhauser and J. Davies, *Electroweak corrections to $gg \rightarrow HH$: Factorizable contributions*, *PoS LL2024* (2024) 014 [[2407.05787](#)].
- [16] M. Bonetti, P. Rendler and W. J. Torres Bobadilla, *Two-loop light-quark Electroweak corrections to Higgs boson pair production in gluon fusion*, *JHEP* **07** (2025) 024 [[2503.16620](#)].
- [17] A. Bhattacharya, F. Campanario, S. Carlotti, J. Chang, J. Mazzitelli, M. Mühlleitner et al., *Higgs-Pair Production via Gluon Fusion: Top-Yukawa- and light-quark-induced electroweak Corrections*, [2512.14823](#).
- [18] M. Bonetti, G. Heinrich, S. Jones, M. Kerner, P. Rendler, T. Stone et al., *Towards the full NLO electro-weak corrections to Higgs boson pair production*, in *2025 European Physical Society Conference on High Energy Physics*, 11, 2025, [2511.15267](#).
- [19] M. Bonetti, G. Heinrich, P. Rendler and W. J. Torres Bobadilla, *NLO QCD corrections to the electroweak production of a Higgs boson pair in the quark-antiquark channel*, [2601.16924](#).

- [20] T. Liu and A. A. Penin, *High-Energy Limit of QCD beyond the Sudakov Approximation*, *Phys. Rev. Lett.* **119** (2017) 262001 [[1709.01092](#)].
- [21] J. Davies, G. Mishima, M. Steinhauser and D. Wellmann, *Double-Higgs boson production in the high-energy limit: planar master integrals*, *JHEP* **03** (2018) 048 [[1801.09696](#)].
- [22] J. Davies, G. Mishima, M. Steinhauser and D. Wellmann, *Double Higgs boson production at NLO in the high-energy limit: complete analytic results*, *JHEP* **01** (2019) 176 [[1811.05489](#)].
- [23] S. Catani, S. Devoto, M. Grazzini, S. Kallweit, J. Mazzitelli and C. Savoini, *Higgs Boson Production in Association with a Top-Antitop Quark Pair in Next-to-Next-to-Leading Order QCD*, *Phys. Rev. Lett.* **130** (2023) 111902 [[2210.07846](#)].
- [24] G. Wang, T. Xia, L. L. Yang and X. Ye, *On the high-energy behavior of massive QCD amplitudes*, *JHEP* **05** (2024) 082 [[2312.12242](#)].
- [25] S. Jaskiewicz, S. Jones, R. Szafron and Y. Ulrich, *The structure of quark mass corrections in the $gg \rightarrow HH$ amplitude at high-energy*, *JHEP* **09** (2025) 015 [[2501.00587](#)].
- [26] Z. Hu, T. Liu and J. M. Yang, *The $gg \rightarrow HH$ amplitude induced by bottom quarks at two-loop level: planar master integrals*, *JHEP* **09** (2025) 132 [[2503.10051](#)].
- [27] Z. Hu and T. Liu, *Double logarithmic contribution to Higgs pair production in the high-energy limit*, [2509.06381](#).
- [28] R. Bonciani, G. Degrossi, P. P. Giardino and R. Gröber, *Analytical Method for Next-to-Leading-Order QCD Corrections to Double-Higgs Production*, *Phys. Rev. Lett.* **121** (2018) 162003 [[1806.11564](#)].
- [29] L. Bellafronte, G. Degrossi, P. P. Giardino, R. Gröber and M. Vitti, *Gluon fusion production at NLO: merging the transverse momentum and the high-energy expansions*, *JHEP* **07** (2022) 069 [[2202.12157](#)].
- [30] J. Davies, G. Mishima, K. Schönwald and M. Steinhauser, *Analytic approximations of $2 \rightarrow 2$ processes with massive internal particles*, *JHEP* **06** (2023) 063 [[2302.01356](#)].
- [31] J. Davies, K. Schönwald, M. Steinhauser and D. Stremmer, *ggxy: A flexible library to compute gluon-induced cross sections*, *Comput. Phys. Commun.* **320** (2026) 109933 [[2506.04323](#)].
- [32] P. Nogueira, *Automatic Feynman Graph Generation*, *J. Comput. Phys.* **105** (1993) 279.
- [33] M. Gerlach, F. Herren and M. Lang, *tapir: A tool for topologies, amplitudes, partial fraction decomposition and input for reductions*, *Comput. Phys. Commun.* **282** (2023) 108544 [[2201.05618](#)].
- [34] B. Ruijl, T. Ueda and J. Vermaseren, *FORM version 4.2*, [1707.06453](#).
- [35] J. Davies, T. Kaneko, C. Marinissen, T. Ueda and J. A. M. Vermaseren, *FORM Version 5.0*, [2601.19982](#).
- [36] R. Harlander, T. Seidensticker and M. Steinhauser, *Complete corrections of Order alpha alpha-s to the decay of the Z boson into bottom quarks*, *Phys. Lett. B* **426** (1998) 125 [[hep-ph/9712228](#)].
- [37] T. Seidensticker, *Automatic application of successive asymptotic expansions of Feynman diagrams*, in *6th International Workshop on New Computing Techniques in Physics Research: Software Engineering, Artificial Intelligence Neural Nets, Genetic Algorithms, Symbolic Algebra, Automatic Calculation*, 5, 1999, [hep-ph/9905298](#).

- [38] G. Mishima, *High-energy expansion of two-loop massive four-point diagrams*, *JHEP* **02** (2019) 080 [[1812.04373](#)].
- [39] H. Zhang, *Massive two-loop four-point Feynman integrals at high energies with AsyInt*, *JHEP* **09** (2024) 069 [[2407.12107](#)].
- [40] M. Fael, K. Schönwald and M. Steinhauser, *A first glance to the kinematic moments of $B \rightarrow X_c \ell \nu$ at third order*, *JHEP* **08** (2022) 039 [[2205.03410](#)].
- [41] R. N. Lee, *Presenting LiteRed: a tool for the Loop InTEgrals REDuction*, [1212.2685](#).
- [42] R. N. Lee, *LiteRed 1.4: a powerful tool for reduction of multiloop integrals*, *J. Phys. Conf. Ser.* **523** (2014) 012059 [[1310.1145](#)].
- [43] P. Maierhöfer, J. Usovitsch and P. Uwer, *Kira—A Feynman integral reduction program*, *Comput. Phys. Commun.* **230** (2018) 99 [[1705.05610](#)].
- [44] J. Klappert, F. Lange, P. Maierhöfer and J. Usovitsch, *Integral reduction with Kira 2.0 and finite field methods*, *Comput. Phys. Commun.* **266** (2021) 108024 [[2008.06494](#)].
- [45] F. Lange, J. Usovitsch and Z. Wu, *Kira 3: integral reduction with efficient seeding and optimized equation selection*, [2505.20197](#).
- [46] A. V. Smirnov and M. Zeng, *FIRE 7: Automatic Reduction with Modular Approach*, [2510.07150](#).
- [47] A. Denner, *Techniques for calculation of electroweak radiative corrections at the one loop level and results for W physics at LEP-200*, *Fortsch. Phys.* **41** (1993) 307 [[0709.1075](#)].
- [48] A. Denner and S. Dittmaier, *Electroweak Radiative Corrections for Collider Physics*, *Phys. Rept.* **864** (2020) 1 [[1912.06823](#)].
- [49] J. Fleischer and F. Jegerlehner, *Radiative Corrections to Higgs Decays in the Extended Weinberg-Salam Model*, *Phys. Rev. D* **23** (1981) 2001.
- [50] S. Dittmaier and H. Rzehak, *Electroweak renormalization based on gauge-invariant vacuum expectation values of non-linear Higgs representations. Part I. Standard Model*, *JHEP* **05** (2022) 125 [[2203.07236](#)].
- [51] A. Sirlin, *Radiative Corrections in the $SU(2)$ -L \times $U(1)$ Theory: A Simple Renormalization Framework*, *Phys. Rev. D* **22** (1980) 971.
- [52] Ancillary files at: <https://www.ttp.kit.edu/preprints/2026/ttp26-006/>.
- [53] J. Davies, G. Mishima, M. Steinhauser and D. Wellmann, *$gg \rightarrow ZZ$: analytic two-loop results for the low- and high-energy regions*, *JHEP* **04** (2020) 024 [[2002.05558](#)].
- [54] W. H. Press, S. A. Teukolsky, W. T. Vetterling and B. P. Flannery, *Numerical Recipes: The Art of Scientific Computing (Third Edition)*. Cambridge University Press, 2007.
- [55] PARTICLE DATA GROUP COLLABORATION collaboration, *Review of particle physics*, *Phys. Rev. D* **110** (2024) 030001.